Lasers in Manufacturing Conference 2025

Development of a predictive control strategy for compensating dimensional errors due to thermal effects in laser tube cutting processes

Bertella L.[1,2], Trivisonno A.[2], Agostini C.[2], Gandolfi D. [2], Pacher M.[2], Moretti G. [1] and Vanin M.[2]

[1]*Dipartimento di Ingegneria Industriale, Università di Trento, Via Sommarive 9, Povo, 38123 Trento (TN), Italy*
[2]*Adige S.P.A., BLM GROUP, Via per Barco 11, 38056 Levico Terme (TN), Italy*

Abstract

Precision in manufacturing has become essential in today's competitive market, necessitating the minimization of all sources of inaccuracies. In the laser cutting process, the inherently thermal nature introduces significant heat to the workpiece, causing thermal expansion and dimensional errors in the absence of compensating strategies. These issues are particularly pronounced in aluminium tube workpieces due to their high thermal conductivity, large expansion coefficient, and extended axial dimensions of the raw material, which amplify thermal expansion effects. This study addresses these challenges by developing a real-time-capable predictive dynamic model. The model correlates commanded laser power with average heat-induced temperature increase, enabling precise, workpiece-specific thermal expansion estimation while maintaining computational efficiency. Calibrated and validated on an industrial laser tube machine, the proposed strategy achieves an average error reduction up to 75%, significantly improving dimensional accuracy and offering a robust solution for high-precision laser-based manufacturing.

Keywords: Laser cutting; Thermal expansion; Thermal errors; Predictive dynamic model.

1. Introduction

Precision manufacturing is essential in today's competitive market, driven by increasing demands for high performance and efficiency (Ramesh et al., 2000a). The primary source of inaccuracy in CNC-machined components is deviation in tool-workpiece motion, with thermal errors being the most significant, accounting for approximately 70% of total errors (Li et al., 2021; Ramesh et al., 2000b).

Laser cutting has emerged as a dominant technology in modern manufacturing due to its unparalleled precision and versatility. Compared to traditional cutting methods (e.g. plasma and waterjet cutting), it offers greater flexibility, faster cutting speeds, and superior cut quality—often producing smooth, clean edges that require little to no post-processing (Steen et al., 2010). Although laser cutting is highly efficient, not all the laser energy is effectively utilized for cutting (Caristan, 2004). A significant portion of the energy is lost from the cutting zone through conduction, convection, and radiation, with conduction being the dominant mode of heat dissipation (Prusa et al., 1999). This heat loss, influenced by the materials properties of the workpiece, results in a rise in the overall material temperature. The consequent thermal expansion can lead to dimensional inaccuracies in the final workpiece, presenting a significant challenge for achieving the required precision.

While heat accumulation in the workpiece is well documented, its direct link to thermal expansion and dimensional errors remains underexplored. Most research emphasizes cut quality degradation, especially in reactive cutting, where exothermic reactions cause unstable heat generation. Levichev et al., 2020 and Busatto et al., 2023 demonstrated this effect using

industrial fiber laser machines and proposed mitigation strategies, with Busatto et al. also incorporating ISO 9013-based quality assessments.

Thermal accumulation is a significant concern also in fusion cutting: despite the heat generated is lower, it can still pose challenges, especially with materials that have high thermal conductivity and high thermal expansion coefficient, such as aluminium. Furthermore, in laser tube cutting machines, the extended axial dimensions of the raw material, combined with the aspiration system, contribute to additional thermal effects. The aspiration system generates an internal airflow to remove cutting smoke and debris, causing heat distribution along the entire tube. As a result, the heat spreads throughout the material, leading to a higher overall temperature increase and, consequently, greater thermal expansion. Finally, the expansion introduces thermal errors, which may compromise the dimensional accuracy of the workpiece.

This work presents a dynamic thermal model for estimating thermal expansion in the laser tube cutting process. The model takes as input the material parameters and commanded laser power, aiming to predict the thermal expansion of the workpiece and compute correction terms that could be used by the CNC controller to compensate for dimensional inaccuracies. The approach was calibrated and validated on Al6060 tubes using an industrial laser tube cutting machine equipped with a 6-kW fiber laser source. The predicted final workpiece length was compared with actual measurements, demonstrating high accuracy. This accuracy suggests that, if compensation were applied based on the model's predictions, a significant reduction in dimensional errors could be achieved, offering a robust solution for high-precision laser-based manufacturing.

2. Modelling

The thermal expansion observed in a tube can be approximated as a one-dimensional phenomenon, since elongation predominantly occurs along the axial direction due to the tube's length being significantly greater than its other dimensions. This simplification enables the use of the linear thermal expansion equation to describe the behavior:

$$\Delta L = L_0 \, \alpha \, \Delta T \tag{1}$$

where ΔL is the thermal expansion, L_0 the initial length of the tube, α is the linear thermal expansion coefficient, and ΔT is the mean temperature variation.

When analysing thermal expansion, it is essential to define the boundary conditions of the material, as these determine whether it is free to expand or mechanically constrained. In a typical laser tube cutting machine, the tube is held in place as illustrated in the schematic in Figure 1. One end is rigidly clamped by the spindle, fully restricting all degrees of freedom. The opposite end is supported by a steady rest, which prevents lateral and rotational movement but allows free axial displacement. Consequently, any thermal elongation accumulates in the cut workpiece, resulting in dimensional inaccuracies.

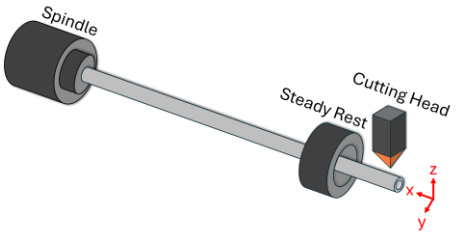

Figure 1: Scheme of a general laser tube machine.

In this study, thermal expansion is analyzed exclusively along the x-axis, consistent with the one-dimensional assumption. Predicting this behavior requires estimating the mean temperature variation along the tube, which is achieved using a thermodynamic model. This model correlates the commanded laser power with the material's thermal response to estimate the temperature distribution.

Given the simplification of the expansion to a one-dimensional case, temperature variations are also assumed to occur only along the tube axis, with changes through the wall thickness and external surface neglected. This assumption is justified by the material's relatively thin walls and high thermal conductivity, which facilitate rapid and uniform heat distribution.

The interaction between the laser and the material is modeled as a moving heat source that travels along the tube axis. This simulates the localized heating effect of the laser. To account for energy losses during the cutting process, the heat input is expressed as a fraction of the commanded laser power.

The temperature dynamic model is developed by performing an energy balance on finite slices of the tube along the x-direction. It incorporates both the thermal behaviour of the tube material—characterized by its cross-section geometry and thermal properties—and the influence inner air. Including the inner air in the model is crucial because, in typical laser tube cutting machines, an internal aspiration system is activated when cutting closed-section tubes. This system generates an airflow from the free end of the tube toward the spindle to evacuate smoke and debris. However, it also significantly affects the thermal profile: while it locally removes heat from the cutting zone, it redistributes thermal energy along the residual bar, resulting in a net increase in the raw material's temperature.

2.1 Thermal balance dynamic equations

Figure 2 presents the scheme of an infinitesimal slice of the tube, illustrated with a circular cross-section for simplicity, though the model is applicable to any closed-section geometry. The thermodynamic model is built upon several simplifying assumptions:

- *Constant properties*: material and internal air properties are assumed constant, regardless of temperature variations.
- *Neglected surface/mass changes*: the model does not account for the progressive detachment of offcut material, assuming constant geometry.
- *Uniform convection*: convective heat transfer coefficients are considered uniform along the tube surfaces.
- *No pressure losses*: internal airflow is assumed to experience negligible pressure drop.
- *Ideal air behaviour*: the internal air is treated as an ideal gas with constant density, ensuring a steady fluid velocity throughout the tube.

The thermal balance for the material considers the system as a closed system where no work is done, and there are no variations in potential or kinetic energy—only heat exchange and accumulation. It is expressed as:

$$m_s c_s \frac{\partial T}{\partial t} = \eta P \delta(x - x_L) \; - A_{cs} k \frac{\partial^2 T}{\partial x^2} \; - A_{ext} h_{ext} (T - T_{amb}) \; - A_{int} h_{int} (T - T_a) \tag{2}$$

where m_s is the mass of the material portion of the slice, c_s is the specific heat capacity of the tube material, T is the tube temperature, η is the fraction of the commanded laser power P converted into heat, $\delta(x - x_L)$ is the Dirac delta function centered at the laser position x_L, A_{cs} is the cross-sectional area of the tube, k is the material thermal conductivity of the material, A_{ext} and A_{int} are the external and internal surface areas of the slice, h_{ext} and h_{int} are the respective convective heat transfer coefficients, T_{amb} is the ambient temperature, and T_a is the temperature of the internal air.

The thermal balance for the inner air is modelled as an open system, where heat exchange, accumulation, and convective transport due to mass flow are considered. It is expressed as:

$$m_a c_{v_a} \frac{\partial T_a}{\partial t} = A_{int} h_{int} (T - T_a) - \dot{m} c_{p_a} \frac{\partial T_a}{\partial x} \tag{3}$$

where m_a is the mass of the inner air of the slice, c_{v_a} is the air specific heat capacity at constant volume, T_a is the temperature of the inner air, A_{int} is the internal surface of the slice, h_{int} is the internal convective coefficient, T is the tube temperature, $\dot{m} = \rho_a A_{cs_{in}} c_a$ is the mass flow rate, ρ_a is the air density, $A_{cs_{in}}$ is the internal cross section of the tube, c_a is the fluid velocity, and c_{p_a} is the air specific heat capacity at constant pressure.

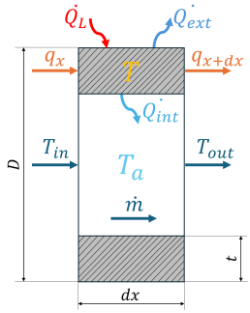

Figure 2: Scheme of the infinitesimal slice of the tube.

The model consists of two coupled partial differential equations, which are solved numerically by approximating the partial derivatives using finite difference method. This requires discretizing the spatial domain with a step size Δx and the temporal domain with a time increment Δt. To ensure numerical stability and accuracy while maintaining computational efficiency, a proper relationship between Δx and Δt must be established.

The strictest stability condition arises from the advective equation (which governs the inner air balance) and is known as the Courant-Friedrichs-Lewy (CFL) condition. This condition is expressed as:

$$\Delta t \leq \frac{\Delta x}{\gamma\, c_a} \tag{4}$$

where $\gamma = \frac{c_{p_a}}{c_{v_a}}$ is the heat capacity ratio of air, c_{p_a} and c_{v_a} are the specific heat capacities of air at constant pressure and volume, respectively, and c_a is the air velocity.

2.2 Thermal expansion prediction

The estimation of temperature profiles allows for the calculation of mean temperature variations and, consequently, the corresponding thermal expansion components. In laser tube cutting, two primary effects influence the final length of the workpiece:

1. *Tube elongation* – As shown in Figure 3 the interaction between the laser and the material increases the mean temperature of both the residual bar and the workpiece. This thermal input causes expansion, affecting the final length of the workpiece in its hot state, expressed as:

$$L_h = L_{wp} + \Delta L_b + \Delta L_{wp_h} \tag{5}$$
$$\Delta \mathrm{L_b} = L_b\, \alpha\, \Delta T_b \tag{5}$$
$$\Delta L_{wp_h} = L_{wp}\, \alpha\, \Delta T_{wp_h} \tag{6}$$

   where L_h is the workpiece length in hot conditions, L_{wp} is the nominal workpiece length, ΔL_b and ΔL_{wp_h} are the thermal expansions of the residual bar and the workpiece, respectively, L_b is the residual bar length, α is the linear thermal expansion coefficient, ΔT_b is the mean temperature variation of the residual bar- before and after the workpiece execution, and ΔT_{wp_h} is the mean temperature variation of the workpiece material, again before and after the workpiece execution.

2. *Shrinkage of the hot workpiece* – After the final cut, the workpiece cools to ambient temperature, resulting in thermal contraction. This shrinkage is described by:

$$L_f = L_h - \Delta L_{wp_c} \tag{8}$$
$$\Delta L_{wp_c} = L_h\, \alpha\, \Delta T_c \tag{9}$$

   where L_f is the final workpiece length at ambient temperature, ΔL_{wp_c} is the shrinkage effect due to cooling, and ΔT_c is the temperature drop from the hot condition to ambient temperature.

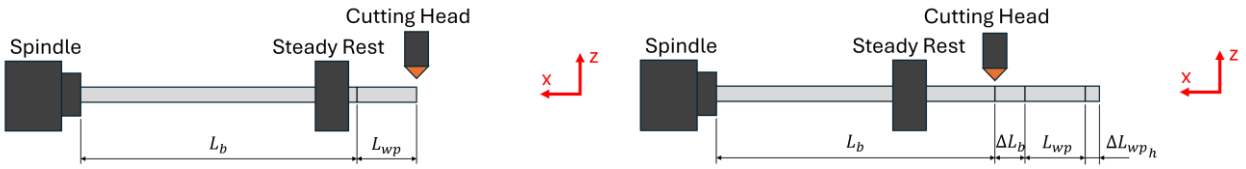

(a) Scheme of a generic initial cut condition. (b) Scheme of a generic final cut condition.

Figure 3: Scheme of the thermal expansion phenomena during laser tube cutting process.

Thermal elongation and shrinkage occur concurrently during cutting, producing a superimposed effect. If the shrinkage during cooling is different from the thermal expansion, the final workpiece may exhibit dimensional inaccuracies.

2.3 Thermal expansion compensation

To improve the dimensional accuracy of the workpieces, a correction must be applied to the x-positioning of the cutting head, as the machine itself does not account for thermal expansion. Figure 4 illustrates the difference between a workpiece cut without compensation and one with the correction applied.

The correction term to be sent to the CNC system is defined as:

$$\Delta L_h = \Delta L_b + \Delta L_{wp_h} \quad (10)$$

$$corr_x = L_{wp} - L_f = -\left(\Delta L_h - \Delta L_{wp_c}\right) \quad (11)$$

where ΔL_h is the total thermal expansion of the tube, and $\mathrm{corr_x}$ is the correction term applied to the cutting head position.

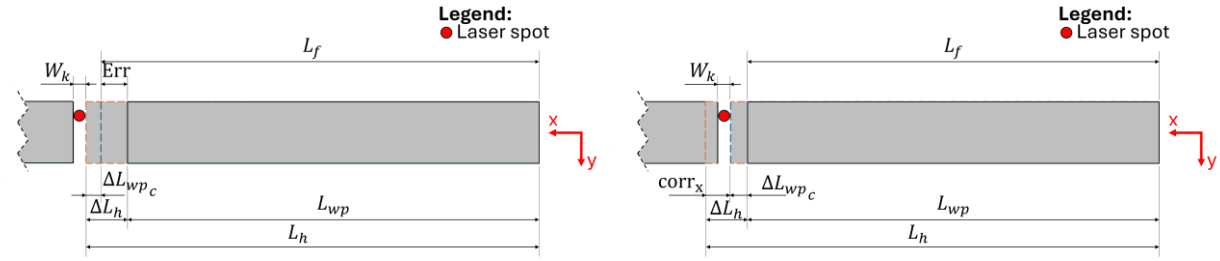

(a) Final cut without compensation. (b) Final cut with compensation.

Figure 4: Comparison between the absence and the presence of thermal expansion compensation.

3. Material and Methods

3.1. Material

The study focuses on aluminium 6060, the most commonly used alloy in laser tube cutting, primarily due to its excellent extrudability (Davim, 2013). The analysed cross-sections include a round tube with a 50 mm diameter and 3 mm thickness, and a square tube with a 50 mm side length and 2 mm thickness. These geometries are widely used in industrial applications, making them ideal candidates for evaluating the effects of thermal expansion and dimensional accuracy in laser cutting processes.

The nominal chemical composition of these batches is shown in Table 1.

Table 1: Nominal chemical composition of Al 6060 (wt%).

Element	Si	Fe	Mn	Mg	Cu	Zn	Cr	Ti	Others	Al
Concentration [%]	0.30	0.10	0.10	0.35	0.10	0.15	0.05	0.10	0.05	balance
	-	-		-					–	
	0.60	0.30		0.60					0.15	

3.2. Laser system

The experiments were performed on a commercial version of the LT8.20 cutting machine (*Adige S.P.A., BLMGroup, Levico Terme, Italy*). An industrial high-power multi-mode fiber laser source that can deliver up to 6 kW of power at a central emission wavelength of $\lambda = 1070\ nm$ (*YLS-6000-CUT, IPG Photonics Coorp., Oxford, Massachusetts*) is employed for the cutting tests. The transport fiber is a graded-index optical fiber having a core diameter of $d_{core} = 50\ \mu m$ and is coupled to a TubeCutter (*Adige S.P.A., BLMGroup, Levico Terme, Italy*) cutting head. The optical process chain is composed of two optical elements, respectively a collimation ($f_{col} = 75\ mm$) and a focusing lens ($f_{foc} = 155\ mm$). From theoretical calculations, the beam waist diameter in the focal position was computed ($d_{waist} \approx 100\ \mu m$).

3.3. Experimental plan

To validate the model, the testing procedure was structured in two phases. In the first phase, a batch of workpieces was cut on the laser cutting machine, during which key data required by the model—such as the x-position of the laser and the commanded power (combination of power and duty cycle)—were logged. In the second phase, this data was used to simulate the cutting scenario using the dynamic model, which provided estimated final workpiece lengths. These predictions were then compared with the actual measured lengths to assess the model's accuracy.

To explore a range of cutting conditions, several critical boundary parameters were varied. The scenarios included different initial tube lengths (ITL), distinct laser power settings (DLP), various cross-sectional geometries, alternative workpiece designs (DWP), and interruptions between successive cuts to simulate loss-of-cut conditions (LOC). The tests configurations are summarized in Table 2, and the workpieces are shown in Figure 5.

For each test, only ten workpieces were cut, as experimental evidence indicated that after this number of cuts, the final workpiece dimensions stabilized. Nitrogen was used as the assist gas during all cutting operations.

Table 2: Experimental design of the different tests done.

Test name	Workpiece	Cross-section	$L_{wp}\ [mm]$	$L_{b_{init}}\ [m]$	P [kW]	Notes
ITL – DLP	Figure 5a	Round	200	3.00; 600	3; 6	
ITL – DLP	Figure 5b	Square	200	5.60; 3.00	3; 6	
DWP	Figure 5c	Square	500	6.15	6	
LOC	Figure 5b	Square	200	6.50; 3.00	3	1 and 4 LOC

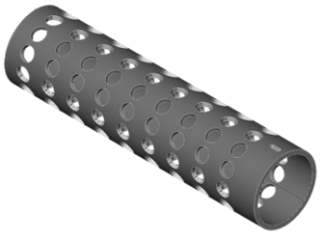

(a) Round tube, diameter 50 mm, thickness 3 mm, length 200 mm.

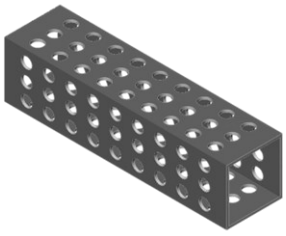

(b) Square tube, side length 50 mm, thickness 2 mm, length 200 mm.

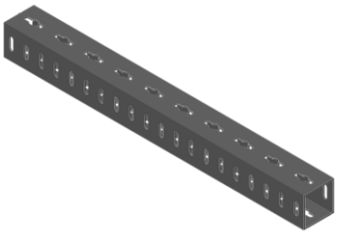

(c) Square tube, side length 50 mm, thickness 2 mm, length 500 mm.

Figure 4: Different workpiece geometries used in the study.

3.4. Characterization and measurement

To quantify the dimensional error caused by thermal expansion and to compare model predictions with experimental data, results are presented as deviations of the workpiece length from its nominal value. Experimental measurements were obtained by taking three axial measurements per workpiece. The final reported value is the mean of these measurements, accompanied by an error bar representing three times the standard deviation.

3.5. Model parameters estimation

The model contains parameters that are not known a priori, such as the fluid velocity (c_a), internal convective coefficient (h_{int}), external convective coefficient (h_{ext}) and the fraction of laser power converted into heat (η). The fluid velocity was measured directly on the machine using a Pitot tube, ensuring proper sensor placement relative to the entry length. The remaining three parameters were identified through a minimization process.

This procedure involved generating a training dataset for each cross-section, consisting of ten cuts of a reference workpiece. To ensure consistency between datasets, the laser power was set to 6 kW and the initial tube length to 6 m. For the round tube, the reference workpiece is shown in Figure 5a, and for the square cross-section, in Figure 5b.

The dataset includes measurements of the first and last workpiece lengths. To improve computational efficiency, the minimization function was designed to simulate only the first cut. However, using only the first workpiece length does not capture the shrinkage effect. This is because the first cut begins and ends at ambient temperature, meaning the thermal expansion of the workpiece material (ΔL_{wp_h}) is fully compensated for its subsequent contraction, effectively canceling out the shrinkage component (ΔL_{wp_c}). To account for shrinkage, the cost function also incorporates the measurement of the last workpiece. This approach relies on the assumption of process repeatability, which implies a consistent shrinkage effect across successive cuts. In the last cut, shrinkage is most pronounced, and the elongation of the residual bar is negligible due to thermal stabilization. Unlike the first cut—where the mean bar temperature increases significantly—the last cut occurs under quasi-steady thermal conditions. Here, the mean bar temperature at the start and end of the cut remains nearly constant, making the contributions of bar elongation (ΔL_b) and workpiece material expansion (ΔL_{wp_h}) negligible. As a result, the dominant term becomes the shrinkage of the cut workpiece (ΔL_{wp_c}), governed by the expression $L_h \; \alpha \; \Delta T_c$. Assuming that the final temperature of each workpiece is consistent across cuts, ΔT_c remains constant. Although L_h may vary slightly, its variation is minimal (maximum of 0.5%), making ΔL_{wp_c} approximately constant. This justifies the use of the last workpiece as a reliable reference in the cost function, as it effectively captures the shrinkage behavior.

The cost function is defined as:

$$\begin{aligned} f_{cost} &= \left(L_{1,measured} - L_{1,model}\right)^2 + \left(L_{10,measured} - L_{10,model}\right)^2 \\ &\cong \left(L_{1,measured} - L_{1,model}\right)^2 + \left(\left|L_{10,measured} - L_{wp}\right| - \Delta L_{wp_{c1,model}}\right)^2 \end{aligned} \qquad (12)$$

where f_{cost} is the objective function to minimize, $L_{1,measured}$ and $L_{1,model}$ are the measured and simulated lengths of the first workpiece, $L_{10,measured}$ is the measured length of the last workpiece, and $\Delta L_{wp_{c1,model}}$ is the shrinkage component of the first simulated workpiece.

The optimized parameter values used for both cross-sections are presented in Table 4.

Table 4: Unknown parameters of the model.

Cross-section	c_a [m/s]	h_{int} [$\frac{W}{m^2 \circ C}$]	h_{ext} [$\frac{W}{m^2 \circ C}$]	η [$-$]
Round	15.6	100.19	2.53	0.28
Square	19.8	150.20	2.53	0.24

4. Results

4.1. Different initial tube length and laser power – round cross section

Figure 6 presents the predicted workpiece lengths compared with the measured values for the round cross-section (reference workpiece shown in Figure 5a). This test investigates the influence of initial tube length variations to evaluate the model's capability to capture the aspiration effect, which contributes to heating of the residual bar. Since thermal expansion is directly influenced by the residual bar length, this dependency is critical. Additionally, tests with varying laser power levels were conducted to assess whether the coefficient η effectively accounts for changes in power and the resulting cutting speed.

The model accurately predicts the decreasing trend in final workpiece length. This behavior is initially driven by significant elongation of the residual bar, which strongly affects the first few workpieces. As cutting progresses and the residual bar shortens, its mean temperature stabilizes, reducing its influence. Consequently, shrinkage becomes the dominant effect, resulting in final workpieces that are shorter than the nominal length.

The average error between predicted and measured lengths is approximately 0.08 mm, with a maximum deviation below 0.2 mm.

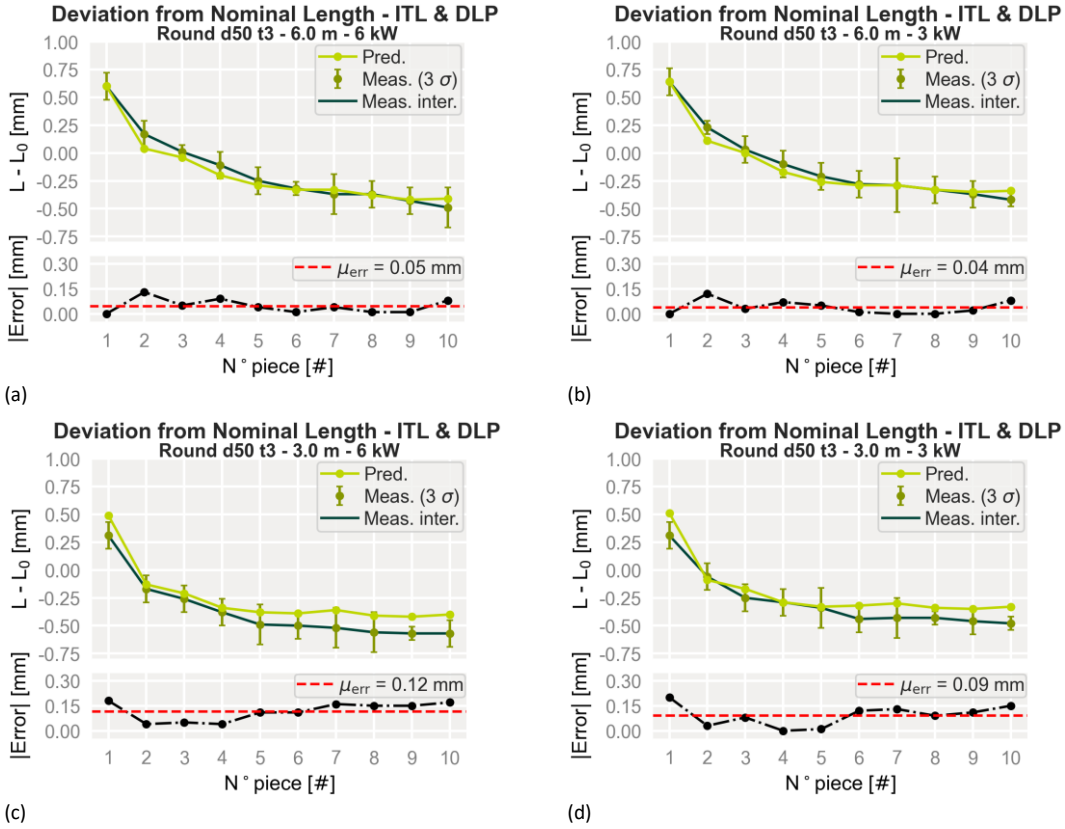

Figure 6: Different initial tube length and laser power – round cross section: (a) $L_{b_{init}} = 6.0\ m$, $P = 6\ kW$; (b) $L_{b_{init}} = 6.0\ m$, $P = 3\ kW$; (c) $L_{b_{init}} = 3.0\ m$, $P = 6\ kW$; (d) $L_{b_{init}} = 3.0\ m$, $P = 3\ kW$.

4.2. Different initial tube length and laser power – square cross section

Figure 7 presents the results of the tests performed on the workpiece shown in Figure 5b, following the same methodology used for the round cross-section. In this case, the differences between the two laser power levels are more pronounced. Notably, higher laser power does not necessarily lead to greater thermal expansion, as seen in the first workpieces of Figures 7a and 7b. This is because laser power directly affects cutting speed—higher power results in shorter cutting time —and thus reduces the amount of energy transferred to the material.

The model accurately predicts the final workpiece lengths, achieving a mean error of 0.05 mm and a maximum error below 0.15 mm. This demonstrates improved accuracy compared to the round cross-section case.

4.3. Generalization

Figure 8 presents the results of the test conducted on a different workpiece, shown in Figure 5c, which features a distinct length and geometry. This test was designed to evaluate whether the estimated unknown parameters were specific to the reference workpieces used during the minimization process or could be generalized.

The model demonstrated strong predictive capability, confirming that the identified parameters are applicable beyond the training geometries. It achieved a mean error of 0.03 mm, with a maximum error below 0.1 mm.

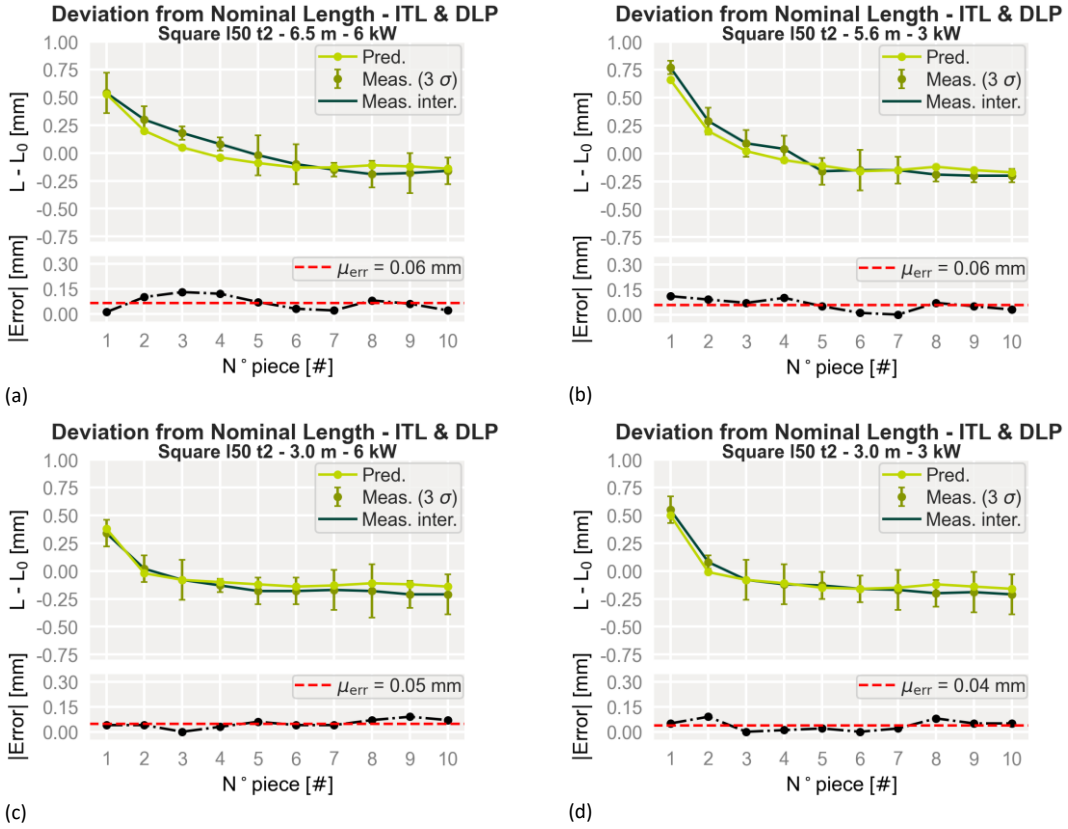

Figure 7: Different initial tube length and laser power – square cross section: (a) $L_{b_{init}} = 6.5\ m$, $P = 6\ kW$; (b) $L_{b_{init}} = 5.6\ m$, $P = 3\ kW$; (c) $L_{b_{init}} = 3.0\ m$, $P = 6\ kW$; (d) $L_{b_{init}} = 3.0\ m$, $P = 3\ kW$.

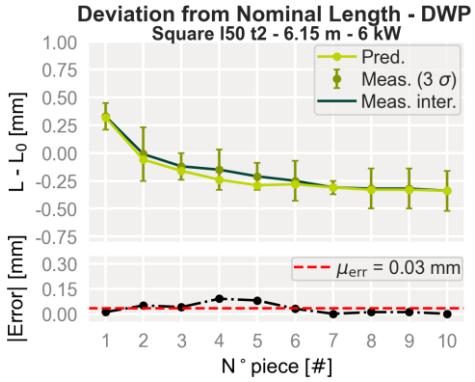

Figure 8: Different workpiece.

4.4. Loss of cut simulations

Figure 9 illustrates the results of the loss-of-cut simulations performed on the workpiece shown in Figure 5b. This test is particularly significant because there are several causes that can halt and resume the cutting process, and one of such is the automatic detection of loss-of-cut (which is a peculiar feature of BLM Group machines). However, during this pause, the aspiration system continues to operate, cooling the tube and significantly altering the initial thermal conditions for the subsequent cut. If the model does not properly account for this effect, its predictions may diverge from actual behavior.

The results clearly indicate the moment at which the loss of cut occurs, as evidenced by a shift in the trend of the final workpiece lengths. This change arises because, upon resuming the cut, the temperature increase is greater than under normal conditions. The model successfully captures this behavior, predicting the final dimensions with a mean error of 0.065 mm and a maximum error below 0.2 mm.

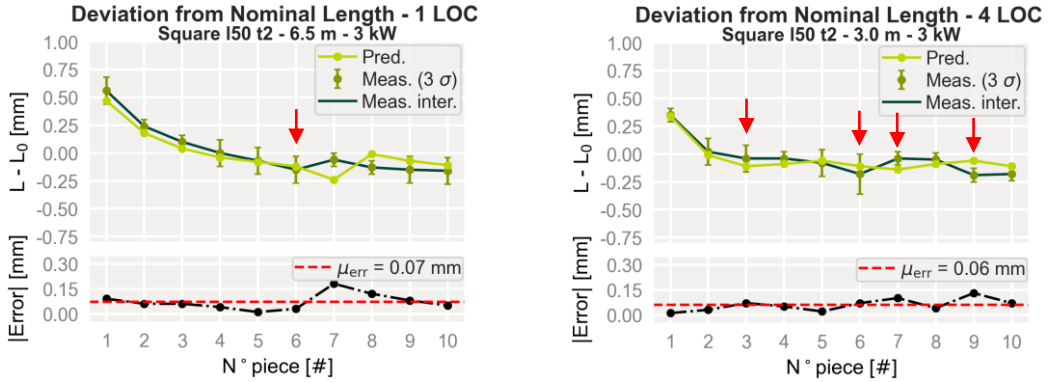

(a) (b)

Figure 8: Loss of cut simulations: (a) 1 Loss of cut simulation; (b) 4 Loss of cut simulation. The loss of cut condition is indicated by the red arrow.

5. Conclusions and future developments

In this study, a predictive model was developed to estimate thermal expansion effects on the dimensional accuracy of workpieces, with a particular focus on aluminium tube cutting processes. The model operates without requiring direct temperature measurements, which are especially challenging for aluminium due to its low emissivity and sensitivity to multiple influencing parameters. A systematic procedure for parameter identification was established, and the model was validated across various cutting conditions, tube cross-sections, and workpiece geometries.

The key findings are that, if the information from the dynamic model for thermal expansion compensation are used:

- It allows for the reduction in the mean dimensional error by up to 75%, lowering the maximum observed error from 0.8 mm to 0.2 mm.
- It eliminates systematic trends in final workpiece lengths, resulting in a distribution more closely centered around the nominal value and demonstrating higher repeatability of the cutting process over the different workpieces in the same batch.

To further enhance the model's robustness and applicability, the following developments are still to be addressed:

- Extension to open cross-sections and a wider range of materials, to validate the model's generalizability.
- Integration of an aspiration system model, enabling fluid velocity estimation through simple measurements on the aspiration side.
- Real-time implementation in industrial settings, allowing dynamic compensation and adaptive control during machining operations.

References

Busatto, M., Caprio, L., Cazzador, M., Vanin, M., & Previtali, B. (2023). *Investigating cut quality degradation due to heat accumulation during the laser cutting of high thickness mild steel plates*.

Caristan, C. L. (A c. Di). (2004). *Laser cutting guide for manufacturing*. Society of Manufacturing Engineers.

Davim, J. P. (2013). *Nontraditional Machining Processes: Research Advances*. Springer London. https://doi.org/10.1007/978-1-4471-5179-1

Levichev, N., Costa Rodrigues, G., Dewil, R., & Duflou, J. R. (2020). Anticipating heat accumulation in laser oxygen cutting of thick metal plates. *Journal of Laser Applications*, *32*(2), 022018. https://doi.org/10.2351/7.0000052

Li, Y., Yu, M., Bai, Y., Hou, Z., & Wu, W. (2021). A Review of Thermal Error Modeling Methods for Machine Tools. *Applied Sciences*, *11*(11), 5216. https://doi.org/10.3390/app11115216

Prusa, J. M., Venkitachalam, G., & Molian, P. A. (1999). Estimation of heat conduction losses in laser cutting. *International Journal of Machine Tools and Manufacture*, *39*(3), 431–458. https://doi.org/10.1016/S0890-6955(98)00041-8

Ramesh, R., Mannan, M. A., & Poo, A. N. (2000a). Error compensation in machine tools—A review. *International Journal of Machine Tools and Manufacture*, *40*(9), 1235–1256. https://doi.org/10.1016/S0890-6955(00)00009-2

Ramesh, R., Mannan, M. A., & Poo, A. N. (2000b). Error compensation in machine tools—A review. *International Journal of Machine Tools and Manufacture*, *40*(9), 1257–1284. https://doi.org/10.1016/S0890-6955(00)00010-9

Steen, W. M., Steen, W. M., & Mazumder, J. (2010). *Laser material processing* (4th ed). Springer.